

Effect of Line Defects on the Electrical Transport Properties of Monolayer MoS₂ Sheet

Amretashis Sengupta, *Member, IEEE*, Dipankar Saha, *Student Member, IEEE*, Thomas A. Niehaus, and Santanu Mahapatra, *Senior Member, IEEE*

Abstract—We present a computational study on the impact of line defects on the electronic properties of monolayer MoS₂. Four different kinds of line defects with Mo and S as the bridging atoms, consistent with recent theoretical and experimental observations, are considered herein. We employ the density functional tight-binding (DFTB) method with a Slater–Koster-type DFTB-CP2K basis set for evaluating the material properties of perfect and the various defective MoS₂ sheets. The transmission spectra are computed with a DFTB-non-equilibrium Green’s function formalism. We also perform a detailed analysis of the carrier transmission pathways under a small bias and investigate the phase of the transmission eigenstates of the defective MoS₂ sheets. Our simulations show a two to four fold decrease in carrier conductance of MoS₂ sheets in the presence of line defects as compared to that for the perfect sheet.

Index Terms—Density functional tight-binding (DFTB), line defects, MoS₂, non-equilibrium Green’s function (NEGF).

I. INTRODUCTION

TWO DIMENSIONAL (2-D) transition metal dichalcogenides, especially MoS₂, have shown great promise as an alternate channel material for next-generation electron devices [1], [2] due to their intrinsic nonzero bandgap, which gives them a distinct advantage over graphene for logic circuit applications. Apart from this, 2-D materials offer enhanced electrostatic integrity, optical transparency, and mechanical flexibility. Thus, a great activity, in both experimental and computational research, has started to understand the electrical properties of atomically thin layered MoS₂ crystals [1]–[8].

Although a number of studies had been conducted on possible enhancement/degradation of MoS₂ electrical properties,

Manuscript received March 26, 2014; revised September 7, 2014; accepted October 15, 2014. Date of publication October 21, 2014; date of current version January 6, 2015. The review of this paper was arranged by Associate Editor Jun Li. This work was supported by the Department of Science and Technology (DST), Government of India, under Grant SR/S3/EECE/0151/2012. The work of A. Sengupta was supported by the DST, Government of India, through the DST INSPIRE Faculty Award DST/INSPIRE/04/2013/000108.

A. Sengupta was with the Nano Scale Device Research Laboratory, Department of Electronic Systems Engineering, Indian Institute of Science, Bangalore 560012, India. He is now with the School of VLSI Technology, Indian Institute of Engineering Science and Technology, Shibpur, Howrah 711103, India (e-mail: dr.a.sengupta@ieee.org).

D. Saha and S. Mahapatra are with the Nano Scale Device Research Laboratory, Department of Electronic Systems Engineering, Indian Institute of Science, Bangalore 560012, India (e-mail: dipsah_etc@yahoo.co.in; santanu@cedt.iisc.ernet.in).

T. A. Niehaus is with the Institute I—Theoretical Physics, University of Regensburg, 93040 Regensburg, Germany (e-mail: thomas.niehaus@physik.uni-regensburg.de).

Color versions of one or more of the figures in this paper are available online at <http://ieeexplore.ieee.org>.

Digital Object Identifier 10.1109/TNANO.2014.2364038

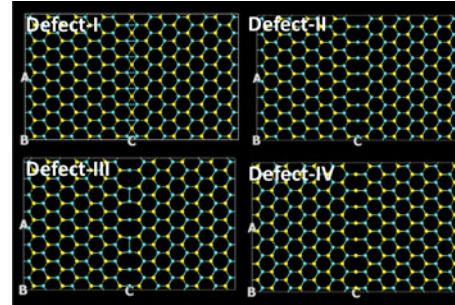


Fig. 1. Various line defects in 2-D MoS₂ considered in our study (top view). A, B, and C denote the supercell axes.

not much focus had given to defects and deformations in MoS₂ sheets. Point defects, dislocations, and grain boundary effects can significantly impact the carrier transport in 2-D MoS₂ channels. Intrinsic crystallographic faults like line defect in single-layer MoS₂ can occur due to stoichiometry changes in the S shell during fabrication. Recently, Enyashin *et al.* [6] have reported experimental results on the various types of line defects present in 2-D MoS₂. However, their report is more focused on defect formation and dynamics, rather than examining how such defects could alter the electrical properties of MoS₂ sheets.

This paper reports a computational study on the impact of such line defects on the electrical transport properties of monolayer MoS₂ sheets. We investigate four different types of line defects with the density functional tight-binding method in QuantumWise ATK [9]. We compute the density of states (DOS), transmission spectra, transmission eigenstates, and the pathways for electron and hole transport in such defective and perfect sheets.

II. METHODOLOGY

Fig. 1 shows the various line defects in sheets of 2-D MoS₂ considered for our studies. We consider a freestanding monolayer MoS₂ flake having a length of 5 nm and a width of 2.5 nm. Such supercell dimensions are considered sufficient for accurately simulating the electronic properties of a periodic sheet of MoS₂ as reported by other groups [10]–[13]. As shown in Fig. 1, the first type of defect henceforth referred to as defect I has two zigzag edges joined in a bridging network of both S and Mo atoms. Defects II and III have only Mo, as the bridging atom. Defect III differs from defect II in the sense of the presence of an additional almost Stone–Wales-type defect in the bridging Mo atoms alternating honeycombs. Defect IV consists of only

S as the bridging atom and does not display any other variants as in defect III. The defects are consistent with the results of Enyashin *et al.*[6].

To calculate the electrical properties of our supercell, we employ DFTB theory in QuantumWise ATK 13.8.0 [9]. We use a $9 \times 1 \times 9$ Monkhorst-Pack k-grid [14] and employ the Slater–Koster-type DFTB-CP2K basis set for MoS₂ available within the ATK package [15], [16]. The transmission spectra and associated parameters such as the transmission eigenstates and the transmission pathways are simulated in QuantumWise ATK using the self-consistent DFTB-NEGF method. This DFTB-NEGF method is chosen for our case as it has been found to yield fast and acceptably accurate simulations for large supercells of transition metal dichalcogenide materials [10]–[13]. In the NEGF method, we proceed to solve the Poisson–Schrödinger equation of the supercells self-consistently. It is assumed that the electrode regions are perfectly ohmic. Setting up the self-energy matrices Σ_L and Σ_R for the left and right contacts, the Green’s function G is constructed as

$$G(E) = [EI - H - \Sigma_S - \Sigma_L - \Sigma_R]^{-1}. \quad (1)$$

In (1), I is the identity matrix, Σ_S is the elastic carrier scattering self-energy matrix, H is the Hamiltonian matrix of the system, and E is the energy eigenvalue. From (1), parameters like the broadening matrices \wp_L and \wp_R and the spectral densities A_L and A_R are evaluated using the following relations:

$$\wp_{L,R} = i[\Sigma_{L,R} - \Sigma_{L,R}^\dagger] \quad (2)$$

$$A_{L,R} = G(E)\wp_{L,R}G^\dagger(E). \quad (3)$$

The density matrix $[\mathfrak{R}]$ used to solve the Poisson equation is given by

$$[\mathfrak{R}] = \int_{-\infty}^{\infty} \frac{dE}{2\pi} [A(E_{k,x})] f_0(E_{k,x} - \eta) \quad (4)$$

where $A(E_{k,x})$ is the spectral density, $E_{k,x}$ is the energy of the conducting level, and η is the chemical potential of the contacts. $f_0(\cdot)$ is the Fermi function. For NEGF studies, a multigrid Poisson solver is employed using Dirichlet boundary conditions on the left and right faces (i.e., the electrodes) and periodic boundary conditions along the width of the supercell. The electrode temperatures are considered 300 K. The carrier density n_{tot} is evaluated from the NEGF formalism and put into the Poisson solver to self-consistently and iteratively evaluate the potential U_{SCF} . The converged values of the carrier density and the self-consistent potential are used to calculate the transmission matrix $\mathfrak{S}(E, V)$

$$\mathfrak{S}(E, V) = \text{trace}[A_L \wp_R] = \text{trace}[A_R \wp_L]. \quad (5)$$

For the transmission spectra, we use the Krylov self-energy calculator [9] with the average Fermi level being set as the energy zero parameter.

The transmission pathways are evaluated by splitting the transmission coefficient into local bond contributions $\mathfrak{S}_{i,j}$. The pathways are such that, if the system is divided into two parts a and b , then the pathways across the boundary between a and b

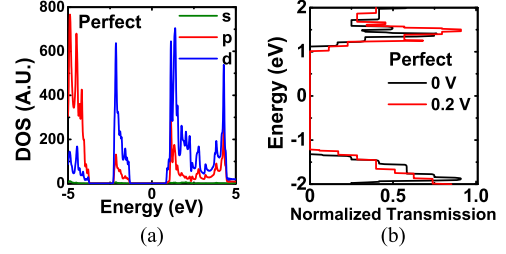


Fig. 2. (a) DOS and (b) Transmission spectra of perfect MoS₂ supercell.

sum up to the total transmission coefficient as [9], [17], [18]

$$\mathfrak{S} = \sum_{i \in a, i \in b} \mathfrak{S}_{i,j}. \quad (6)$$

The transmission contribution of local bonds, $\mathfrak{S}_{i,j}$, could be both positive and negative. A negative value physically signifies that the electron is being back scattered along the bond. The pathways are represented with colored arrows representing the direction and the magnitude of the contributions by each of the local paths, in comparison to one another.

To find the transmission eigenstates of the sheet, we use the following methodology. The transmission matrix can be expressed as [9], [19], [20]

$$\mathfrak{S}_{nm} = \sum_k t_{nk} t_{km}^\dagger. \quad (7)$$

In (7), the transmission amplitude from Bloch state ψ_n in the left electrode to Bloch state ψ_k in the right electrode is represented by t_{nk} and that from the Bloch state ψ_k in the right electrode to Bloch state ψ_m in the left electrode is represented by t_{km}^\dagger . The transmission coefficient is given by the trace of the transmission matrix $\mathfrak{S} = \sum_n \mathfrak{S}_{nn}$. The Bloch states can be expressed in a linear combination

$$\sum_n \ell_{\alpha,n} \psi_n \quad (8)$$

and the transmission eigenstates are evaluated by the diagonalization of the transmission matrix by $\ell_{\alpha,n}$

$$\sum_m \mathfrak{S}_{nm} \ell_{\alpha,m} = \lambda_\alpha \ell_{\alpha,n} \quad (9)$$

with transmission eigenvalue λ_α .

III. RESULTS AND DISCUSSIONS

In Fig. 2(a) and (b), we show the DOS and the normalized transmission spectra of the perfect MoS₂ sheet under consideration. From Fig. 2(a), a forbidden gap of 1.84 eV is estimated between the valence band (VB) maxima and conduction band (CB) minima of the material. This is in accordance with reported bandgap of 1.78 eV of perfect MoS₂ sheets [10]–[13]. The most significant contributions to the DOS come from the p and d orbitals of Mo and S atoms. If we see the normalized transmission spectra for the perfect sheet as in Fig. 2(b), we find two distinct peaks at 1.5 and -1.68 eV. Upon the application of a small bias of 0.2 V (on either the left or right electrode keeping the other terminal grounded), we observe the edges of the transmission

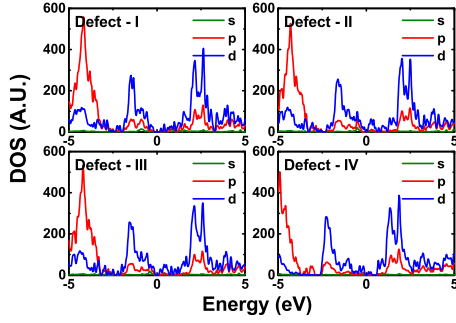


Fig. 3. DOS of various types of line defects in MoS₂ sheets. Defect states contributions are seen in the region near the Fermi level (set at zero).

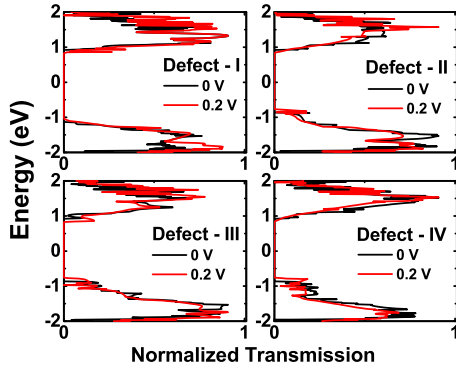


Fig. 4. Transmission spectra under zero-bias and a low applied bias (0.2 V) condition for the various types of line defects in MoS₂ sheets. The change in the transmission spectra is independent of the choice of bias terminal.

spectra drawing slightly closer to the Fermi level. This signifies availability of a greater number of conducting channels both in CB and VB.

In Fig. 3, we have the DOS of the various defective sheets under consideration. Here, we observe the states to be more evenly spread out, having much less sharper peaks in the DOS compared to perfect MoS₂ sheet. The defect states are seen to exist in considerable density even in the formerly forbidden gap of the perfect MoS₂. This indicates the possibility of a semiconductor to semi-metal transition (depending on the contribution of these defect states to the carrier transmittance) of the MoS₂ sheets in the presence of the line defects. From the transmission spectra in Fig. 4 of the various defective sheets, we observe that the staircase like behavior of the spectra (as seen for the perfect sheet) no longer persists and the defect states near the Fermi level (as seen in the DOS plots) do not contribute much to the number of transmission channels. In case of a perfect sheet, the symmetry is preserved and the degeneracy of energy levels leads to a staircase behavior; in case of line defects, the symmetry is broken and the energy degeneracy is lost, thus leading to a smearing (loss of step-wise nature) of the transmission spectra.

It should be noted that the transmission spectra shown in Fig. 4 have been normalized in order to gain a better understanding of the relative contribution of various energy bands to the total transmission spectra of the MoS₂ sheets. We show

mostly the region near the Fermi level of the spectra, since for small bias, this is the most significant part of the transmission spectra that contributes to carrier transport. With a small applied bias on either left/right terminal of the sheets, the contributions of the various available channels seem to undergo some minor redistribution. Under such bias, the transmission peaks, signifying most transparent channels for carrier conduction for defect I, are observed at 1.33 and -1.88 eV. For defect II, the peaks are at 1.56 and -1.92 eV; for defect III, these are 1.54 and -1.72 eV; and for defect IV, the peaks are at 1.54 and -1.74 eV, respectively.

In our studies, we consider the elastic scattering in the channel for electron/hole transport. Therefore, it is of interest to look into the transmission eigenstates and the transmission pathways for the defective sheets. In order to visualize the transmission eigenstates and pathways, we select the energy values corresponding to maximum transmission (as in Fig. 4) for each case. For the electron transmission eigenstates and the transmission pathways, the energy state corresponding to the transmission peak on the CB is considered. For the hole transmission, it is the energy state corresponding to the transmission peak on the VB that is considered.

The phase isosurface plots of the transmission eigenstates shown in Fig. 5(a) and (b) are for those energies corresponding to the peak of the transmission spectra on the CB side (for electrons) and VB side (for holes) in Fig. 4. A quantum transmission eigenstate can be considered to be made up of superposition of two different states, one of which corresponds to the electron/hole moving from the left electrode to the right electrode and another due to the electron/hole moving from the right electrode to the left electrode. This is mathematically represented in (7). The relative phase of those two states has a value, which depends on the distance from each of the two electrodes. Depending upon this, an interference-like pattern may emerge in the overall isosurface plot which is quite symmetric/periodic in case of the perfect sheet. For defective sheets, the pattern turns out more or less chaotic/random due to the symmetry breaking, depending upon the scattering from the defect. Only in case of defect II, we observe a certain amount of phase shift across the defect (about $\frac{\pi}{2}$ for electron transmission states and $\frac{3\pi}{4}$ for hole transmission states) in the pattern in an otherwise random plot. This locally symmetric pattern in the vicinity of the defect II is arising out of the superposition of the transmission states conducting the carriers in the two opposite directions (left to right and the right to left electrodes). In the other defect cases, the interference is not happening in such a way so as to produce any fixed amount of phase shift across the line defect. It is defect I that seems to have most random nature of the phase isosurface plots, followed by defects IV and III. The high degree of randomization in the phase of the transmission eigenstates due to the defects can signify lesser coherence of transmission states across the defective sheets, which can suppress their overall conductance.

The electron and hole transmission pathways for the perfect and defective sheets are presented in Fig. 6(a) and (b). The pathways shown here are calculated corresponding to the states with the maximum transmission (as in Fig. 4) for each

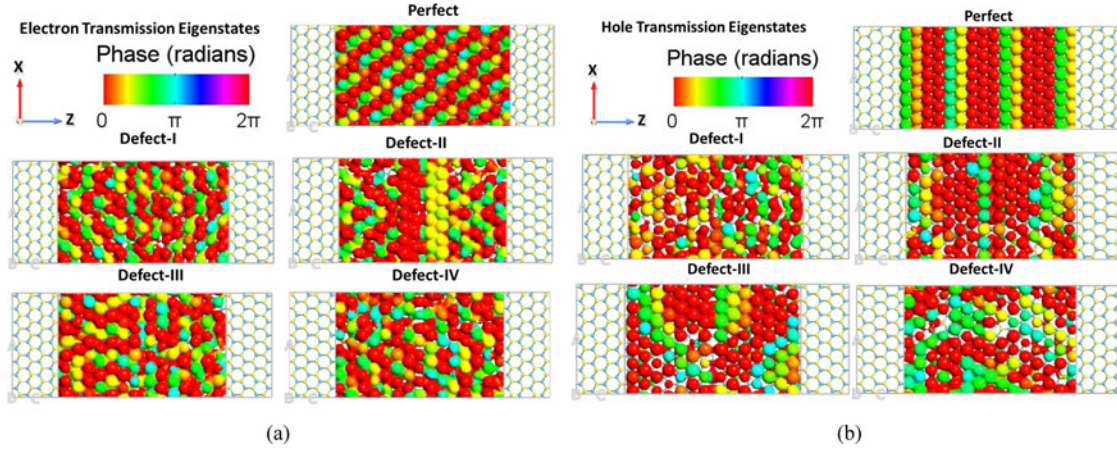


Fig. 5. (a) Electron and (b) hole transmission eigenstates isosurface plots for the perfect and the various defective sheets. Isosurfaces are plotted for an applied bias of 0.2 V, at the CB transmission peak for electrons and VB transmission peak for holes.

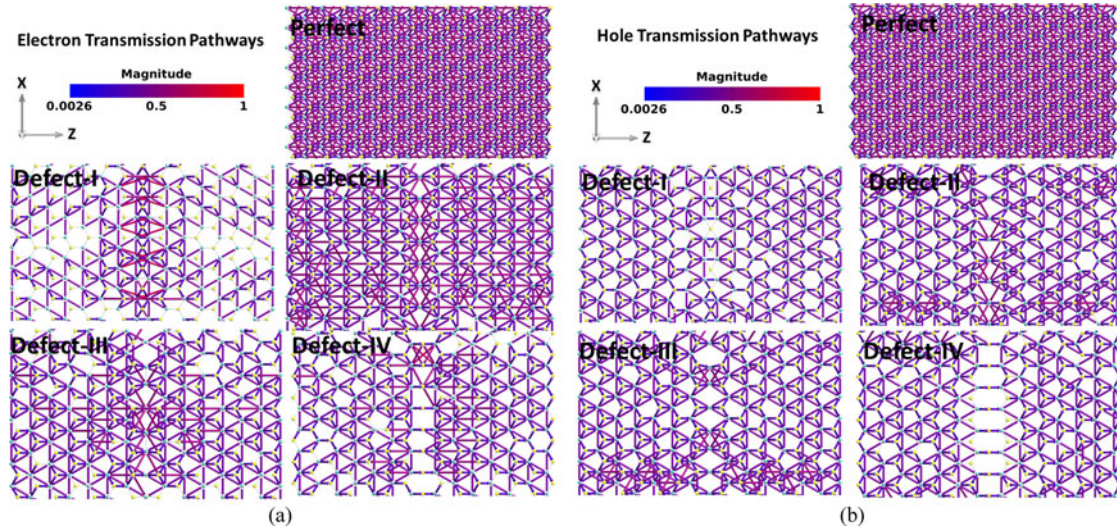


Fig. 6. (a) Electron and (b) hole transmission pathways plotted for an applied bias of 0.2 V, at the CB transmission peak for electrons and VB transmission peak for holes. The pathways are represented with colored arrows representing the direction and the magnitude of the contributions by each of the local paths, in comparison to one another.

(perfect and defective) case. The pathways are represented with colored arrows representing the direction and the magnitude of the contributions by each of the local paths, in comparison to one another. The transmission is scaled as $\frac{t}{t_{max}} \times p$, with p being the scaling power. The value of p is taken to be 0.01. For clarity, a threshold value (minimum bond-length considered for the plotting a path) was taken 0.05 Å. As for the magnitude is considered, the local transmission magnitude for each pathway is color coded (red corresponding to a relative magnitude of 1.0 and blue to a relative magnitude of 0.026). The relative scale factor and the threshold values are kept the same for all the pathway plots. From the plots, we see that the pathways for electron and hole transmission at the respective CB and VB transmission peaks are identical in case of perfect sheet of MoS₂. This is in accordance with the closely matching values of electron and hole effective masses for perfect MoS₂ sheets as reported in our earlier work [21]. However, for the line defects, the transmission

pathways differ significantly for electrons and holes. Also for the line defect case, we see that much lesser number of paths for both electrons and holes are available in general for transmission compared to the perfect sheets. For majority of the electron and hole transmission local pathways, the color of the arrows varies between violet to purple, which corresponds to relative magnitudes in the range of 0.25–0.75.

In defect I, the number of available transmission paths near the defect site seems more for electron transport compared to that for hole transport; also, the magnitude of transmission through these pathways is higher compared to that for the holes. In defect I, the transmission path between the Mo atoms around the line defect has the highest magnitude of electron conductance as seen in Fig. 6(a). The same pathways do not seem equally conducive to hole transport, as evident from Fig. 6(b). However, away from the defect site, there exist lesser number of paths for electrons than that for holes in defect I.

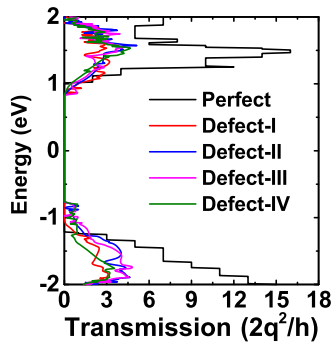


Fig. 7. Absolute transmission under low-bias (0.2 V) condition.

For defect II also, there exist a larger number of paths near the defect for electron transport than that for hole transport. Same is observed for defects III and IV. Overall in all the defects, we observe some highly electron conducting paths between the metallic atoms (Mo–Mo) around the defects. However, for hole transport, this route does not offer any enhanced carrier transport and is equivalent in transport magnitude to the Mo–S pathway in case of holes. The S–S pathway is weakly conducive in either electron or hole transport.

In Fig. 7, we show the absolute value of transmission spectra of the perfect and the various defective sheets under a small applied bias of 0.2 V. It is worth mentioning here that the transmission spectra shown earlier in Figs. 2(b) and 4 are normalized to provide a better view of how the relative contribution of various energy bands to the total transmission of the channel (MoS₂ sheet) evolve under applied bias. In order to understand the carrier conductance through the channel, it is the absolute value of the transmission that is more significant than the normalized $\Im(E, V)$. As seen in Fig. 7, the magnitude of transmission through the perfect sheet is significantly larger than that for the defective ones. The defect states have a slight contribution to transmission near the energy levels of 1 and -1 eV, whereas the transmission for the perfect sheet in these regions is somewhat lesser. Also, for the defective sheets, the levels are less discrete and do not have the staircase behavior as in the perfect sheet. At the corresponding transmission peaks, the value of $\Im(E, V)$ for the perfect sheet is two to four times that of the various defective sheets. This indicates a high degree of suppression of carrier transmission in presence of the line defects in MoS₂ sheet.

IV. CONCLUSION

Here, we report the impact of four different types of line defects on the electrical transport properties of monolayer MoS₂ sheets. The defects with different configurations and Mo and S as the bridging atoms, based on recent experimental evidence, are studied with the DFTB-NEGF formalism for their transport behavior.

Our studies show that although a moderate amount of defect states are induced near the Fermi level due to these line defects, the carrier transport through these defect states is rather limited and the overall transmission is highly scattered in the presence of these line defects. We also observe significant defect-induced randomization in the phase isosurface plots of the transmission

eigenstates, leading to loss of coherent transport to a certain degree. The suppression of transmission in the defective sheets and the onset of elastic scattering at the defect centres were also evident from the transmission pathways. Our studies show a sizeable decrease in carrier conductance in MoS₂ sheets due to the presence of line defects as compared to that for the perfect sheet. Such results are very significant considering the future application of MoS₂ monolayer sheets for nanoscale devices.

REFERENCES

- [1] B. Radisavljevic, A. Radenovic, J. Brivio, V. Giacometti, and A. Kis, "Single-layer MoS₂ transistors," *Nat. Nanotechnol.*, vol. 6, no. 3, pp. 147–150, Mar. 2011.
- [2] B. Radisavljevic, M. B. Whitwick, and A. Kis, "Integrated circuits and logic operations based on single-layer MoS₂," *ACS Nano*, vol. 5, no. 12, pp. 9934–9938, Dec. 2011.
- [3] S. K. Mahatha, K. D. Patel, and K. S. R. Menon, "Electronic structure investigation of MoS₂ and MoSe₂ using angle-resolved photoemission spectroscopy and ab-initio band structure studies," *J. Phys. Cond. Matter*, vol. 24, no. 47, pp. 475504-1–475504-5, Oct. 2012.
- [4] X. Li, J. T. Mullen, Z. Jin, K. M. Borysenko, M. Buongiorno Nardelli, and K. W. Kim, "Intrinsic electrical transport properties of monolayer silicene and MoS₂ from first principles," *Phys. Rev. B*, vol. 87, no. 11, pp. 115418-1–115418-9, Mar. 2013.
- [5] W. Bao, X. Cai, D. Kim, K. Sridhara, and M. S. Fuhrer, "High mobility ambipolar MoS₂ field-effect transistors: Substrate and dielectric effects," *Appl. Phys. Lett.*, vol. 102, pp. 042104-1–042104-4, Jan. 2013.
- [6] A. N. Enyashin, M. Bar-Sadan, L. Houben, and G. Seifert, "Line defects in molybdenum disulfide layers," *J. Phys. Chem. C*, vol. 117, no. 20, pp. 10842–10848, Apr. 2013.
- [7] P. Lu, X. Wu, W. Guo, and X. C. Zeng, "Strain-dependent electronic and magnetic properties of MoS₂ monolayer, bilayer, nanoribbons and nanotubes," *Phys. Chem. Chem. Phys.*, vol. 14, no. 37, pp. 13035–13040, Oct. 2012.
- [8] I. Popov, G. Seifert, and D. Tomnek, "Designing electrical contacts to MoS₂ monolayers: A computational study," *Phys. Rev. Lett.*, vol. 108, no. 15, pp. 156802-1–156802-5, Apr. 2012.
- [9] QuantumWise Atomistix ToolKit (ATK). [Online] Available: <http://www.quantumwise.com/> 2014
- [10] G. Seifert, H. Terrones, M. Terrones, G. Jungnickel, and T. Frauenheim, "Structure and electronic properties of MoS₂ nanotubes," *Phys. Rev. Lett.*, vol. 85, no. 1, pp. 146–149, Jul. 2000.
- [11] E. Erdogan, I. H. Popov, A. N. Enyashin, and G. Seifert, "Transport properties of MoS₂ nanoribbons: Edge priority," *Eur. Phys. J. B*, vol. 85, pp. 33-1–33-4, Jan. 2012.
- [12] M. Ghorbani-Asl, S. Borini, A. Kuc, and T. Heine, "Strain-dependent modulation of conductivity in single layer transition-metal dichalcogenides," *Phys. Rev. B*, vol. 87, no. 23, pp. 235434-1–235434-6, Jun. 2013.
- [13] M. Ghorbani-asl, A. N. Enyashin, A. Kuc, G. Seifert, and T. Heine, "Defect-induced conductivity anisotropy in MoS₂ monolayers," *Phys. Rev. B*, vol. 88, no. 24, pp. 245440-1–245440-7, Dec. 2013.
- [14] H. J. Monkhorst and J. D. Pack, "Special Points for Brillouin-zone integrations," *Phys. Rev. B*, vol. 13, no. 12, pp. 5188–5192, 1976.
- [15] CP2K Consortium. [Online]. Available: <http://www.cp2k.org/> 2014
- [16] J. C. Slater and G. F. Koster, "Simplified LCAO method for the periodic potential problem," *Phys. Rev.*, vol. 94, no. 6, pp. 1498–1524, Jun. 1954.
- [17] K. W. Jacobsen, P. Stoltze, and J. K. Nørskov, "A semi-empirical effective medium theory for metals and alloys," *Surface Sci.*, vol. 366, no. 2, pp. 394–402, 1996.
- [18] G. C. Solomon, C. Herrmann, T. Hansen, V. Mujica, and M. A. Ratner, "Exploring local currents in molecular junctions," *Nature Chem.*, vol. 2, pp. 223–228, Feb. 2010.
- [19] A. L. Yeyati and M. Büttiker, "Scattering phases in quantum dots: An analysis based on lattice models," *Phys. Rev. B*, vol. 62, no. 11, pp. 7307–7315, Sep. 2000.
- [20] H. Bouchiat, Y. Gefen, S. Guéron, G. Montambaux, and J. Dalibard, *Nanophysics: Coherence and Transport*. Amsterdam, The Netherlands: Elsevier, 2005, pp. 499–531.
- [21] A. Sengupta, R. K. Ghosh, and S. Mahapatra, "Performance analysis of strained monolayer MoS₂ MOSFET," *IEEE Trans. Electron. Dev.*, vol. 60, no. 9, pp. 2782–2787, Sep. 2013.



Amretashis Sengupta (M'10) received the Ph.D. (Engg.) degree from Jadavpur University, Kolkata, India, in 2012.

He is currently an Assistant Professor at the Indian Institute of Engineering Science and Technology, Shibpur, Howrah, India. His research interests include 2-D material-based FET and atomistic simulations.

Dr. Sengupta received the DST INSPIRE Faculty award from the Department of Science and Technology, Government of India, in 2013.



Thomas A. Niehaus received the Ph.D. (Dr. rer. nat.) degree in physics from the University of Paderborn, Paderborn, Germany in 2001.

After heading a research group at the Bremen Center for Computational Materials Science from 2006 to 2010, he moved to the University of Regensburg, where he is currently a Professor for theoretical physics. His group is working on large-scale first principles simulations of optoelectronic and energy conversion materials, with a recent focus on 2-D materials.



Dipankar Saha (S'12) received the M.Tech. degree from Jadavpur University, Kolkata, India, in 2013. He is currently working toward the Ph.D. degree with Nano Scale Device Research Laboratory, Department of Electronic Systems Engineering, Indian Institute of Science, Bangalore, India.

His research interests include electrothermal transport in nanoelectronic devices and modeling and simulation of nanoscaled devices with 2-D channel materials.



Santanu Mahapatra (M'08–SM'10) received the Ph.D. degree from the Ecole Polytechnique Federale de Lausanne, Lausanne, Switzerland, in 2005.

He is currently an Associate Professor at the Indian Institute of Science, Bangalore, India.

Prof. Mahapatra was a recipient of the Ramanna Fellowship from the Department of Science and Technology, Government of India, for his contribution in compact modeling, in 2012.